processes

MDPI

Article

Caffeine and Paracetamol Adsorption and Antibacterial Activity Using Granular Activated Carbon Modified with Silver and Copper Compounds

Luiza Carla Augusto Molina [1], Jayana Freitas Resende [1], Jumara Silva de Sousa [1], Luis Fernando Cusioli [1], Letícia Nishi [1], Sandro Rogerio Lautenschlager [2] and Rosangela Bergamasco [1,*]

[1] Department of Chemical Engineering, State University of Maringá, Maringá 87020-900, PR, Brazil; lcm.lcam@gmail.com (L.C.A.M.); jayana.freitas@hotmail.com (J.F.R.); pg55425@uem.br (J.S.d.S.); lfcusioli@uem.br (L.F.C.); leticianishi12@gmail.com (L.N.)
[2] Department of Civil Engineering, State University of Maringá, Maringá 87020-900, PR, Brazil; srlager@uem.br
* Correspondence: rbergamasco@uem.br

Abstract

Adsorption is a promising solution to the presence of contaminants in water resources that involves the use of adsorbent materials, such as granular activated carbon (GAC) and nanoparticles like silver (Ag) and copper (Cu). However, the practical challenge of using pure GAC lies in its susceptibility to biofouling. This study aimed to develop a multifunctional GAC/AgCu nanocomposite to address the dual challenge of pharmaceutical contamination and bacterial activity of Escherichia coli. Characterization by SEM, XRF, XRD and FTIR confirmed the successful impregnation of nanoparticles. Kinetic studies showed that the pseudo-first-order model was more suitable for both caffeine and paracetamol contaminants. The Langmuir model provided the best fit for isotherms, achieving maximum adsorption capacities of 138.35 mg g^{-1} for caffeine and 92.21 mg g^{-1} for paracetamol. In antibacterial tests, GAC/AgCu achieved a bacterial reduction of over 97%, whereas pure GAC showed no inhibitory effect, confirming that the antimicrobial properties are derived from the Ag and Cu nanoparticles. These results highlight GAC/AgCu as a promising multifunctional material for the simultaneous removal of emerging pharmaceutical pollutants and biological contaminants, offering a solution to mitigate biofouling and enhance water treatment efficiency.

Keywords: adsorption; antibacterial activity; emerging contaminants; granular activated carbon; metal nanoparticles

Check for updates

Academic Editor: George Z. Kyzas

Received: 25 February 2026
Revised: 16 March 2026
Accepted: 17 March 2026
Published: 21 March 2026

Copyright: © 2026 by the authors. Licensee MDPI, Basel, Switzerland. This article is an open access article distributed under the terms and conditions of the Creative Commons Attribution (CC BY) license.

1. Introduction

Water management and quality are essential for maintaining biological, geological, and chemical cycles that sustain environmental balance. The presence of pharmaceuticals in water resources, resulting from the direct or indirect disposal of pharmaceutical residues, has become an increasingly relevant issue due to the potential adverse effects of these substances on human health and the environment [1]. These compounds are displaced into the environment in several ways, the three main ones being: industrial waste, biological excretion and inappropriate disposal of unused medicines [2]. Wastewater and sewage treatment plants are critical pillars of wastewater management; however, these facilities are not designed specifically for the removal of pharmaceuticals and, therefore, often fail to eliminate these compounds before discharging their effluents [3,4].

Amidst pharmaceuticals, paracetamol, also known as acetaminophen, is one of the most widely used analgesic/antipyretic drugs worldwide because it is safe and does not pose a risk of dependence or significant side effects [5]. The compound has a half-life in aquatic environments of approximately 12.2 days [6] and when consumed 2–5% of the administered dose is not altered by the body and is then excreted in the urine [7]. Due to the high level of consumption, this excretion, combined with industrial and domestic waste, results in the presence of paracetamol in surface waters and sewage systems in several regions of Europe [8–10], India [11], Nigeria [12], China [13], and Brazil [14] in concentrations that reach 0.045 mg L^{-1}. Another highly consumed drug is caffeine, which is the most widely used psychoactive substance in the world, with an average global consumption of approximately 70 mg per person. Approximately 1–10% of the administered dose is excreted in urine and reaches water bodies through sewage, food, beverages, or medications [15,16]. Discarded caffeine first reaches sewage and then wastewater treatment plants. Residual caffeine, which is not biodegradable or is not destroyed during treatment at the treatment plant, enters the water cycle and can mix with drinking water, since caffeine has a stable state in aquatic environment with a half-life reported of 100–240 days [17]. The presence of caffeine and its metabolites in surface waters have already been detected in countries such as India [18], Mexico [19], European countries [10,20,21], Brazil [14,22], and others, with concentrations reaching up to 0.083 mg L^{-1}.

The occurrence of paracetamol in the aquatic environment can cause hepatotoxicity and nephrotoxicity in aquatic organisms, leading to the death of these animals and, consequently, impacting the upper levels of the food chain [5]. In addition to animals, chronic exposure to paracetamol also has toxic effects on plants, such as inhibiting their growth and metabolic activities, affecting their feeding behavior and reproductive capacity [23,24]. When the edible part of crops is polluted with paracetamol, consumers are indirectly consuming all the compounds accumulated in the plant. Furthermore, three studies reported that caffeine exposure (0.5–18.0 mg L^{-1}) for 28 days caused, respectively, 8, 12, and 22% mortality in *Hediste diversicolor*, *Diopatra neapolitana*, and *Arenicola marina* [25–27]. Other biological effects related to the presence of caffeine residues have been observed, such as the induction of inflammation in mollusks [28] and the alteration of microbial communities in insects [29].

Considering this challenge, adsorption emerges as a promising solution to mitigate these issues, offering an efficient and cost-effective approach to the treatment of contaminated water [1]. This method involves the use of adsorbent materials, such as activated carbon (AC), which stands out for its natural origin and properties that facilitate the removal of organic compounds and microorganisms [30,31]. Generally, AC is modified to generate additional functional groups on its surface to enhance receptor sites and improve the contaminant removal process [5]. Furthermore, AC alone is not capable of fully removing bacteria, viruses, or protozoa, requiring functionalization to enhance its properties and achieve applicability in this regard [32].

In the literature, metallic nanoparticles have shown excellent results, with high adsorption capacities for dyes [33], heavy metals [34], ions [35], antibiotics [36,37], caffeine [38], and paracetamol [39], among other contaminants. Moreover, the antimicrobial properties of metallic nanoparticles have been addressed by various researchers, demonstrating satisfactory inactivation rates [40–43]. However, the low particle size of nanoparticles is a major challenge. As a result, their applications in the adsorption process end up being restricted due to the separation of the suspended powder in the batch adsorption process and the compaction of the fixed bed column [44]. Therefore, it is necessary to use a material with larger particle size, such as granular activated carbon (GAC), to support metallic nanoparticles that have smaller particle sizes [45,46]. Furthermore, while post-treatment

disinfection (e.g., UV radiation or chlorination) is standard in wastewater treatment plants, the practical challenge of using GAC lies in its susceptibility to biofouling [47,48]. The accumulation of microbial biofilms on the carbon surface tends to clog pores, drastically reducing the effective surface area for chemical adsorption [48]. Therefore, developing a multifunctional GAC with intrinsic antimicrobial properties is not intended to replace final disinfection, but rather to preserve the material's adsorptive capacity and extend its operational lifespan by inhibiting uncontrolled microbial growth within the filter bed.

While previous studies have separately addressed GAC modification or antimicrobial activity, there is a lack of comprehensive research on GAC/AgCu composites that target both the removal of organic micropollutants and the inhibition of biological proliferation. In this context, the objective of this study was to evaluate the efficiency of the adsorption process as a mechanism for removing caffeine and paracetamol in batch tests, as well as to investigate its potential antibacterial activity against *E. coli*. Thus, this study consisted of synthesizing granular activated carbon modified with silver and copper nanoparticles with the aim of developing a multifunctional adsorbent with potential application in water treatment.

2. Materials and Methods

2.1. Materials

GAC used as a matrix for impregnation was supplied by Purific (Maringá, Brazil). The impregnation compounds silver nitrate ($AgNO_3$, purity $\geq$ 99.0%) analytical grade and copper sulphate ($CuSO_4 \cdot 5H_2O$, purity $\geq$ 98.0–102.0%) analytical grade was purchased by Labsynth Ltd.a (São Paulo, Brazil).

For the synthetic solutions containing pharmaceutical contaminants, caffeine ($C_8H_{10}N_4O_2$, purity $\geq$ 99%) and paracetamol ($C_8H_9NO_2$, purity $\geq$ 99%) were purchased by Purifarma (Maringá, Brazil). The microorganism tested for antibacterial activity was the strain of the bacterium *E. coli* ATCC 25922.

2.2. Production of Granular Activated Carbon Impregnated with Silver and Copper Compounds GAC/AgCu

GAC was used for the incorporation of Ag and Cu nanoparticles via an adapted incipient wetness impregnation method [49]. The GAC was impregnated in a batch reactor using separate aqueous solutions of $CuSO_4$ and $AgNO_3$ at a 1:1 (*w*/*v*) GAC/distilled water ratio, with precursor amounts calculated to achieve target concentrations of 0.06 wt% Ag and 1.0 wt% Cu relative to the dry GAC mass. To enhance the diffusion of metallic compounds into the carbon matrix, the mixture underwent vacuum impregnation at 66.66 kPa and 80 °C for 40 min. Subsequently, the sample was subjected to thermal treatment in a muffle furnace (Model JP7010, JUNG, Blumenau, Brazil) at 350 °C for 5 h under ambient atmosphere and pressure (101.325 kPa).

2.3. X-Ray Diffraction (XRD)

XRD analysis was carried out on the D8 Advance X-ray equipment (Bruker, TX, USA), using Cu-Kα radiation (λ = 1.5406 Å). The crystal structure of the samples was analyzed at a scan rate of 1° 2θ/min, acquisition time of 1 s and angle of incidence varying between 3° and 80° (2θ).

2.4. Brunauer–Emmett–Teller Surface Area Analysis (BET)

The Brunauer–Emmett–Teller (BET) method was applied using an Autosorb analyzer (Model NOVA 1200e, Anton Paar QuantaTec Inc., Boynton Beach, FL, USA). The adsorption and desorption isotherms were utilized to determine the probable textural properties of the functionalized adsorbent materials.

2.5. Transmission Electron Microscopy (TEM)

TEM studies were performed using electron microscopy (Model JEM-1400, JEOL Ltd., Tokyo, Japan). Samples of both GAC and GAC/AgCu were prepared by dispersing and sonicating the granulated samples in ethanol. A drop of the resulting suspension was placed onto a copper grid coated with a formvar/carbon thin film (250 mesh, FCF 200-Cu, EMS). The grid was then allowed to air-dry before being introduced into the microscope column for analysis.

2.6. Scanning Electron Microscopy (SEM)

The morphology of the porous and surface structures of the samples of both GAC and GAC/AgCu was examined by SEM (Model Shimadzu SS-550, Shimadzu Corporation, Kyoto, Japan) operating with a 15 kV electron source, after *Au*-recovering. SEM enables direct observation of surface microstructure changes in the activated carbon samples resulting from the impregnation and thermal decomposition processes.

2.7. Fourier-Transform Infrared Spectroscopy (FTIR)

For the FTIR analysis, a Thermo Fisher Scientific Inc. spectrophotometer (Waltham, MA, USA) was used, operating in the 400 to 4000 cm^{-1} wave number range, to evaluate the functional groups present in the adsorbents. The samples were pelletized with potassium bromide (*KBr*) (Sigma-Aldrich, MI, USA) in a ratio of 1:200 (*w*/*w*).

2.8. X-Ray Fluorescence (XRF)

The XRF analysis was carried out on a Shimadzu model EDX-720 energy-dispersive X-ray fluorescence spectrometer (Shimadzu, Kyoto, Japan) for qualitative analysis. The spectrometer has an X-ray tube with a rhodium (*Rh*) anode, operating in a range from 5 to 50 kV and a current between 1 and 1000 μA. The GAC and GAC/AgCu samples were analyzed within the maximum limits of 300 mm in diameter and 150 mm in height.

2.9. Zeta Potential and Point of Zero Charge (pH_{PZC})

Zeta potential measurements were performed to determine the surface electrostatic charges of GAC and GAC/AgCu using a Beckman Coulter Delsa Nano Zeta analyzer (Shimadzu, Kyoto, Japan). Samples (0.01 g in 10 mL of deionized water) were equilibrated under stirring (150 rpm) at 298 K for 24 h before analysis. The medium pH varied from 2 to 10 by addition of 0.01 M HCl or NaOH. Electrophoretic light scattering was employed to assess the pH-dependent charge stability of the dispersions.

The pH_{PZC} was determined using 0.2 g of GAC/AgCu in aqueous solutions of *NaCl* (0.1 M) with different pHs (2–10) by addition of 0.01 M HCl or NaOH. The suspensions were stirred (150 rpm) at 298 K for 24 h. Then, the final pH values of each were noted and the difference between initial pH and final pH were plotted against the initial pH.

2.10. Adsorption Experiments

The experiments were conducted in batch mode using a shaker table (Model TecnalTE-424, Tecnal, Piracicaba, Brazil) with a stirring speed of 150 rpm, pH 7 and a constant temperature of 298 K for 24 h. For this purpose, sealed recipients were used with 30 mL of pharmaceutical contaminant (caffeine and paracetamol) solution at 30 mg L^{-1} with tap water. All tests were performed in duplicate. The effect of the GAC/AgCu dosage was evaluated using 0.01–0.05 g of GAC/AgCu. The effect of pH (4.0, 7.0, and 10.0) was studied using the best GAC/AgCu mass. After the contact time, the samples were filtered through 0.45 μm qualitative cellulose acetate membranes (UNIFIL, Brazil) and final contaminant concentration readings were taken using a spectrophotometer (Model DR6000-01-RBC, HACH, Loveland, CO, USA) at a wavelength of 273 nm and 242 nm for caffeine and

paracetamol, respectively. The optimum conditions were determined in relation to the adsorption capacity q_e (Equation (1)).

$$q_e = \frac{C_0 - C_e}{m} V, \quad (1)$$

where C_0 is the initial concentration of contaminant (mg L^{-1}), C_e is the equilibrium concentration of the solution (mg L^{-1}), V is the volume of the solution (L), and m is the mass (g) of GAC/AgCu.

Evaluation of *Ag* and *Cu* leaching was performed to evaluate the release of modifiers from the adsorbent. A total of 30 mL of tap water remained 24 h in contact with GAC/AgCu adsorbent (150 rpm, pH 7, 298 K), then the solution was filtrated and used for the analysis. The analyses were carried out by atomic absorption spectrometry (AAS) in a spectrometer (Varian, AA240FS, Santa Clara, CA, USA) at the characteristic wavelength of 328.1 nm for *Ag* and 324.7 nm for *Cu* using air-acetylene flame. The method exhibited a detection limit of 0.1 mg L^{-1} for *Ag* and 1.0 mg L^{-1} for *Cu*.

Furthermore, to analyze the reusability of the adsorbent, 6 cycles of adsorption-desorption were carried out for each contaminant. The GAC/AgCu was recovered from the adsorption experiment through filtration and oven-dried at 60 °C. Then, the desorption test was performed with 30 mL of tap water on a shaker table for 24 h and the material was dried at 60 °C for use in the next cycle.

2.11. Kinetic Study

The kinetic study was conducted at a constant stirring speed of 150 rpm and temperature of 298 K, using 30 mL of contaminant solution at 30 mg L^{-1} and total contact times of 300 min for caffeine and 420 min for paracetamol, which were sufficient to achieve equilibrium. To understand the kinetic mechanism, the pseudo-first-order [50] and pseudo-second-order models were applied [51].

Linear version of the pseudo-first-order equation is expressed as below:

$$\ln(q_e - q(t)) = \ln(q_e) - \ln(k_1\, t), \quad (2)$$

where $q(t)$ is the adsorption capacity of adsorbate at time t (mg g^{-1}), q_e is the adsorption capacity at equilibrium (mg g^{-1}), t is the reaction time (min), and k_1 is the adsorption pseudo-first-order rate constant (min^{-1}).

The linear pseudo-second-order model is represented by:

$$\frac{t}{q(t)} = \frac{1}{q_e^2 k_2} + \frac{t}{q_e}, \quad (3)$$

where k_2 is the adsorption pseudo-second-order rate constant (g mg^{-1} min^{-1}).

2.12. Equilibrium and Thermodynamic Study

Finally, to study the adsorption equilibrium and the effect of temperature on the process, three different temperatures were used (298, 308, and 318 K) with contaminant concentrations ranging from 5 to 100 mg L^{-1}. The tests were conducted using 30 mL of contaminant solution, shaking speed of 150 rpm. Three models of isotherms were applied: Langmuir [52], Freundlich [53] and Temkin [54], all expressed by Equations (4)–(6), respectively.

$$\frac{C_e}{q_e} = \frac{1}{k_L q_{mL}} + \frac{1}{q_{mL}} C_e, \quad (4)$$

$$\ln(q_e) = \ln(k_F) + \frac{1}{n_F} \ln(C_e), \quad (5)$$

$$q_e = \frac{RT}{b_T} \ln(k_T C_e), \tag{6}$$

where q_{mL} represents the maximum adsorption capacity of an adsorbent in the Langmuir model (mg g^{-1}), k_L is the empirical constant of the Langmuir equation related to energy of adsorption (L mg^{-1}), k_F $\left((mg\ g^{-1}) / (mg\ L^{-1})^{n_F} \right)$ and n_F are the Freundlich constant and the adsorption intensity, respectively, b_T is the Temkin constant related to the heat of adsorption (J mol^{-1}) and k_T is the Temkin isotherm constant ($L\ mg^{-1}$).

After the equilibrium study, the data were used to calculate the thermodynamic parameters: Gibbs free energy, enthalpy and entropy through Equations (7)–(9) below:

$$k_d = \frac{q_e}{C_e}, \tag{7}$$

$$\Delta G^\circ = -R\ T\ ln(k_d), \tag{8}$$

$$ln(k_d) = \frac{\Delta S^\circ}{R} - \frac{\Delta H^\circ}{RT}, \tag{9}$$

where R (8.314 J $mol^{-1}K^{-1}$) is the general gas constant, T (K) is the temperature in kelvin, k_d is the distribution coefficient, ΔG° (J mol^{-1}) is the difference in Gibbs free energy variation, ΔH° (J mol^{-1}) is enthalpy difference and ΔS° (J mol^{-1}) denotes entropy variation.

2.13. Antibacterial Tests

The experiments were conducted in batch on a shaker table (Model TecnalTE-424, Tecnal, Piracicaba, Brazil) with a stirring speed of 150 rpm and a constant temperature of 308 K for 24 h. Hermetically sealed recipients were used with 30 mL bacterial contaminant solution. For this purpose, a bacterial suspension of 106 CFU/mL of *E. coli* ATCC 25922 was added in sterile deionized water and Mueller Hilton Broth culture medium. Next, the masses of 0.01 g, 0.03 g, and 0.09 g of GAC and GAC/AgCu were added. A positive control containing the bacterial inoculum and the culture medium was used for each test. The viability of the *E. coli* was determined by the optical density method at a wavelength of 600 nm (OD600). The removal of pathogens in the experiments was evaluated and reliably detected in the drinking water.

The antibacterial activity of the adsorbent was represented as a percentage reduction compared to the control, which was calculated using equation below:

$$\%Bacterial\ reduction = \frac{\left(OD_i - OD_f \right) \times 100}{OD_i}, \tag{10}$$

where OD_i and OD_f are the initial and final optical density, respectively.

3. Results and Discussion

3.1. Characterization of GAC and GAC/AgCu

The textual characterization using N_2 adsorption and desorption data allows the evaluation of the BET specific surface area (S_{BET}), micropore area (S_m), pore volume (V_p), and average pore diameter (d_p) for GAC and GAC/AgCu samples.

The results presented in Table 1 indicate a reduction in surface area, micropore area, and pore volume following the impregnation process. These findings are consistent with the literature, suggesting that the nanoparticles present on the GAC surface may have caused a reduction in area and volume. Conversely, the average pore diameter showed a slight increase, although both samples remained predominantly microporous. This behavior may be related to the vacuum impregnation process, which can increase pore diameter due to the influence of system pressure [34,55,56]. Furthermore, Figure 1 shows the isotherms of

adsorption and desorption of nitrogen at 77 K for the adsorbents. According to IUPAC classification, both isotherms are classified as a Type I configuration, which represents the monolayer adsorption on microporous materials with relatively small external surfaces. Thus, the amount of nitrogen adsorbed by GAC/AgCu was lower compared to GAC. This behavior may be related to the presence of modifier nanoparticles on the material's surface, which may have caused blockage of the pores or adsorption sites, hindering the access and diffusion of N_2 molecules.

Table 1. BET analyses parameters of GAC and GAC/AgCu samples.

Parameters	GAC	GAC/AgCu
S_{BET} $(m^2\ g^{-1})$	1054	730
S_m $(m^2\ g^{-1})$	907	624
V_p $(cm^3\ g^{-1})$	0.46	0.38
d_p (nm)	1.72	2.09

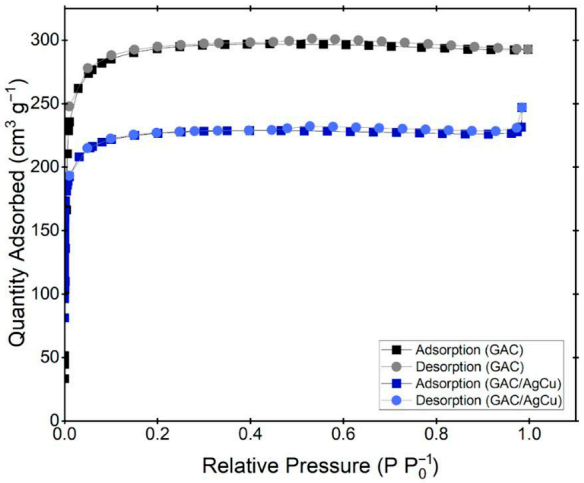

Figure 1. Nitrogen adsorption isotherms for GAC and GAC/AgCu.

The XRD spectra in Figure 2 provides a detailed analysis of the structural differences between GAC and GAC/AgCu. GAC showed broad, diffused peaks, characteristic of a predominantly amorphous structure. These peaks, generally located in the vicinity of 2θ around 24° and 44°, which correspond to the (002) and (101) diffraction planes of typical graphite structure, are indicative of carbonaceous materials with low crystallinity [57–59]. GAC/AgCu showed new, well-defined peaks of greater intensity, showing the crystallinity of the incorporated nanoparticles. A diffraction peak is observed at 2θ near 26.01°, attributed to the (002) plane of graphitic carbon [34,58], confirming the amorphous nature of activated carbon. Furthermore, additional diffraction peaks were detected at 2θ = 39.8° and 64.1°, which correspond to the (111) and (220) planes for silver in metallic form [49,60]. In addition, peaks located near 32.0°, 48.7°, and 53.3°, which are attributed to the crystallographic planes (110), (202), and (020), respectively, indicate the presence of monoclinic CuO [61]. In this respect, the coexistence of Ag and CuO phases in the XRD shows that these nanoparticles were incorporated into the surface of GAC.

For the morphological characterization, the GAC and GAC/AgCu were characterized by TEM (Figure 3) and SEM (Figure 4). In Figure 3a, the overall appearance of the GAC is consistent with a dense, high-surface-area carbon material, where only the morphology is observed. Figure 3b shows a relatively large carbon structure with scattered dark spots throughout the background with a rod-like shape that was not noticed in the non-modified

GAC analysis. Furthermore, the contrast shown in Figure 3c,d displays dark spots scattered on the surface of the adsorbent, associated with silver and copper nanoparticles [41].

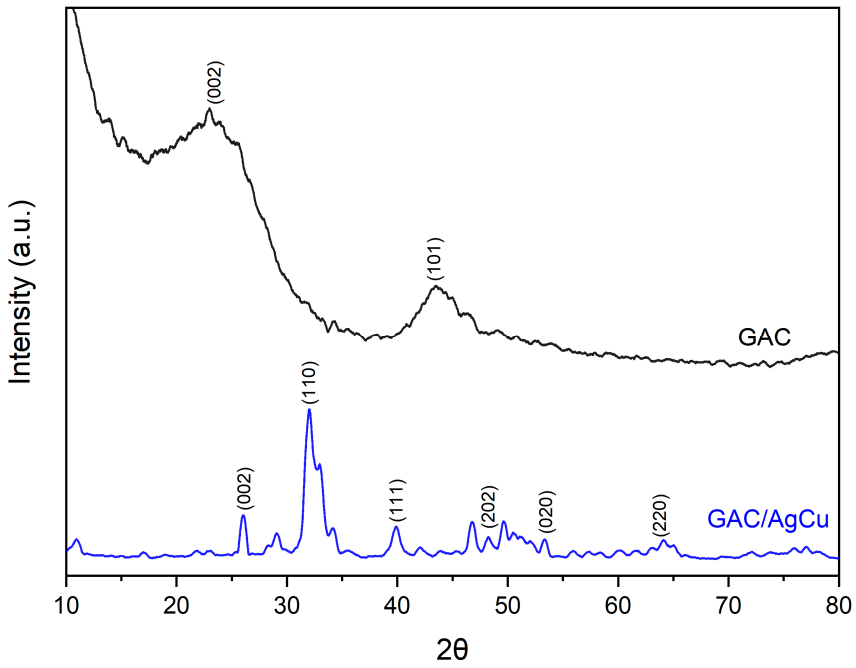

Figure 2. X-ray diffractograms of GAC and GAC/AgCu.

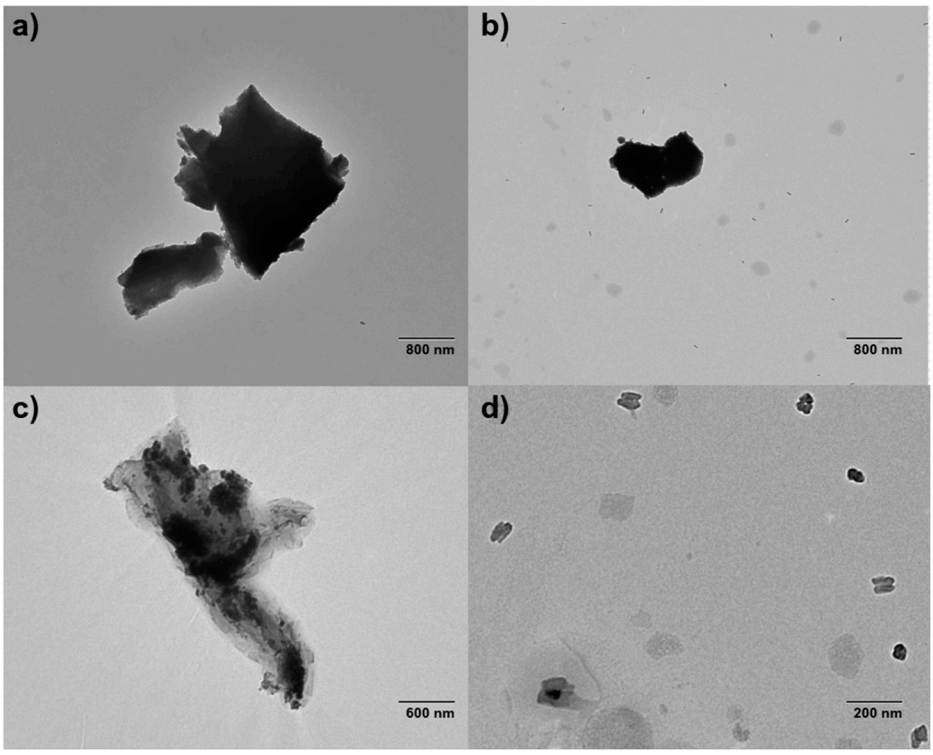

Figure 3. TEM photomicrographs of GAC ((**a**), 800 nm) sample and GAC/AgCu sample ((**b**), 800 nm), ((**c**), 600 nm), ((**d**), 200 nm).

The images presented in Figure 4 show SEM analysis. Figure 4a,b reveals the porous structure of the unmodified GAC. The pores appear with a relatively uniform and well-distributed arrangement, exhibiting an internal tubular shape. The structure suggests a well-preserved hierarchical porosity, typical of high-surface-area activated carbons used in

adsorption processes [30,62–64]. In comparison, Figure 4c,d displays significant changes in surface morphology on the GAC after vacuum impregnation and thermal decomposition, leading to a noticeable increase in surface roughness and the presence of particle deposition within and around the pores. TEM analysis confirms the presence of nanoparticles, which is consistent with the observed changes in the SEM images. Furthermore, the porous structure is less uniform, with some regions appearing collapsed or filled, due to the impregnation process and the presence of modifiers partially filling or blocking the pores [34,65]. It is worth mentioning that the pores identified in the SEM images represent the macroscopic surface morphology and the entrance to the internal pore network. While SEM micrographs revealed a rugged surface with visible macropores (around 5–10 nm) acting as channels for molecular diffusion, the nitrogen isotherm analysis confirmed a predominantly microporous internal structure, which is the primary contributor to the high surface area and adsorption performance.

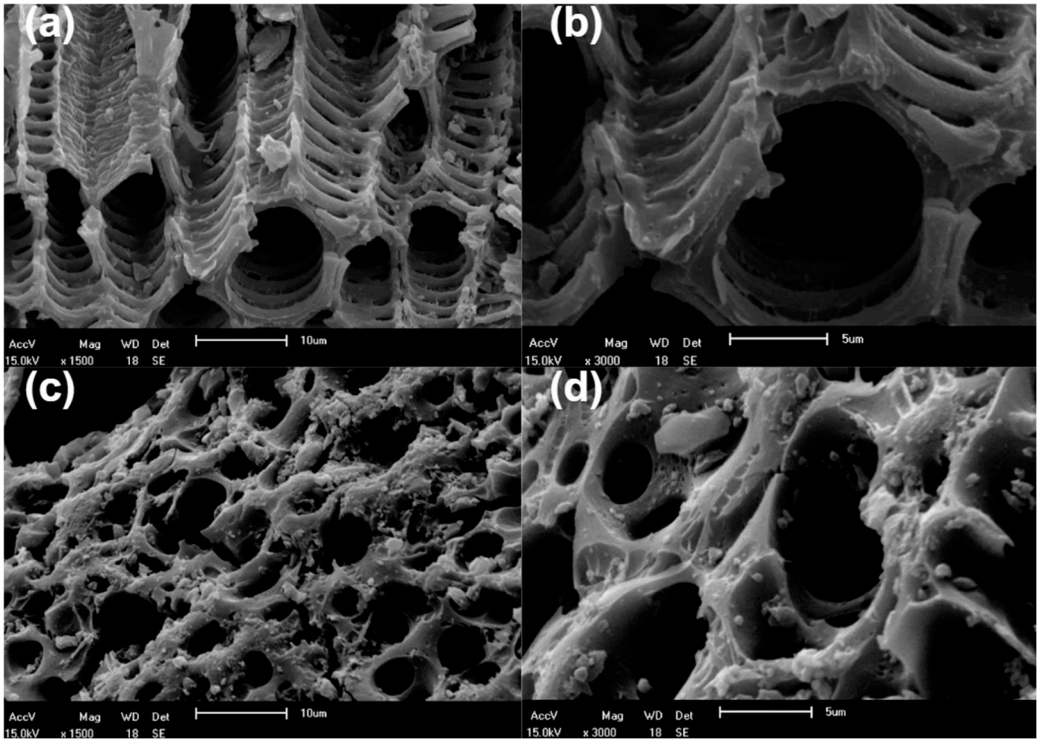

Figure 4. SEM images obtained from GAC sample (**a**,**b**) and GAC/AgCu sample (**c**,**d**).

Figure 5 shows the X-ray fluorescence spectra obtained for the samples analyzed. In Figure 5a, the low-intensity peak in the region characteristic of copper (Cu-Kα, ~8 keV) suggests residual presence of copper in GAC, possibly due to natural impurities or traces of the original material. Furthermore, in Figure 5b no significant peaks were detected in the region corresponding to the emission of silver (Ag-Kα, ~22 keV), indicating the absence of silver in GAC sample or its presence in concentrations below the detection limit of the equipment. Meanwhile, the peak at ~8 keV shown in Figure 5c has a substantially higher intensity compared to that of GAC, suggesting the incorporation of copper into the adsorbent surface after the modification process. This significant presence of copper is compatible with the chemical treatment carried out on the sample. Finally, in Figure 5d, the well-defined peak at ~22 keV corresponds to the characteristic emission of silver (Ag-Kα). The high intensity signal confirmed the incorporation of silver into the structure of the modified adsorbent. Thus, the intense peaks seen in Figure 5c,d prove that the modification process was effective in incorporating copper and silver into the GAC.

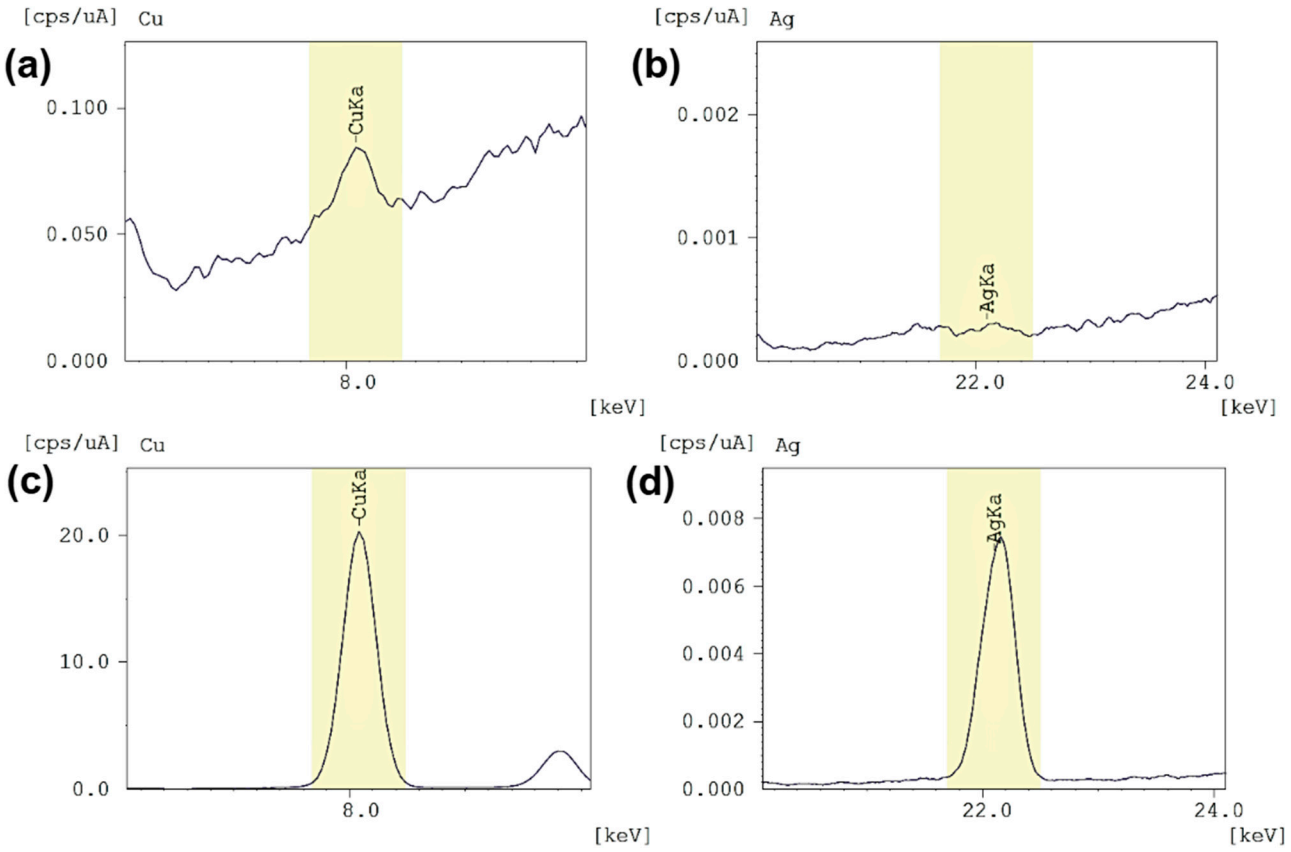

Figure 5. XRF spectra for the elements copper and silver of GAC sample (**a**,**b**), and GAC/AgCu sample (**c**,**d**).

Figure S1 shows the FTIR spectra of the different adsorbent samples before and after modification with silver and copper. In the spectrum of GAC, bands of functional groups typical of the carbon matrix can be seen. The broad band around 3400 cm^{-1} is attributed to the stretching vibrations of hydroxyl groups (-OH), associated with surface functional groups or the presence of adsorbed water molecules [59,66]. Another significant peak occurs at 1600 cm^{-1}, related to the stretching vibrations of C=C groups in aromatic rings, indicating the presence of aromatic structures [67]. In addition, bands in the 1100–1200 cm^{-1} region are attributed to C-O stretching, suggesting the presence of ethers or alcohols on the surface [1]. These results confirm the amorphous and functionalized nature of GAC. In the modified carbon (GAC/AgCu), an attenuation in the intensity of the band at 3400 cm^{-1} was observed, which may be associated with the interaction between the metals and the hydroxyl groups present on the surface of the material [68]. Furthermore, the band at 1600 cm^{-1} showed a slight change in intensity and position, suggesting a possible interaction between the modifiers and the aromatic groups of the carbon matrix [59]. These changes indicate chemical and structural modification of GAC.

3.2. Adsorption Experiments Results

Leaching tests were performed to evaluate the structural stability of the GAC/AgCu nanocomposite. The results demonstrated high chemical stability, as the release of *Ag* and Cu ions remained below the detection limits of 0.1 mg g^{-1} and 1.0 mg g^{-1}, respectively. These findings confirm that the nanoparticles are strongly anchored to the activated carbon matrix, minimizing the risk of secondary contamination.

The pH of the solution represents an important parameter in inorganic and organic compounds adsorption. Therefore, pHs of 4.0, 7.0 and 10.0 were used in this study to

ascertain its influence on both caffeine and paracetamol adsorption capacity by GAC/AgCu. Figure 6 shows the influence of pH on adsorption experiments on GAC/AgCu, zeta potential analysis results and the determination of pH_{PZC}.

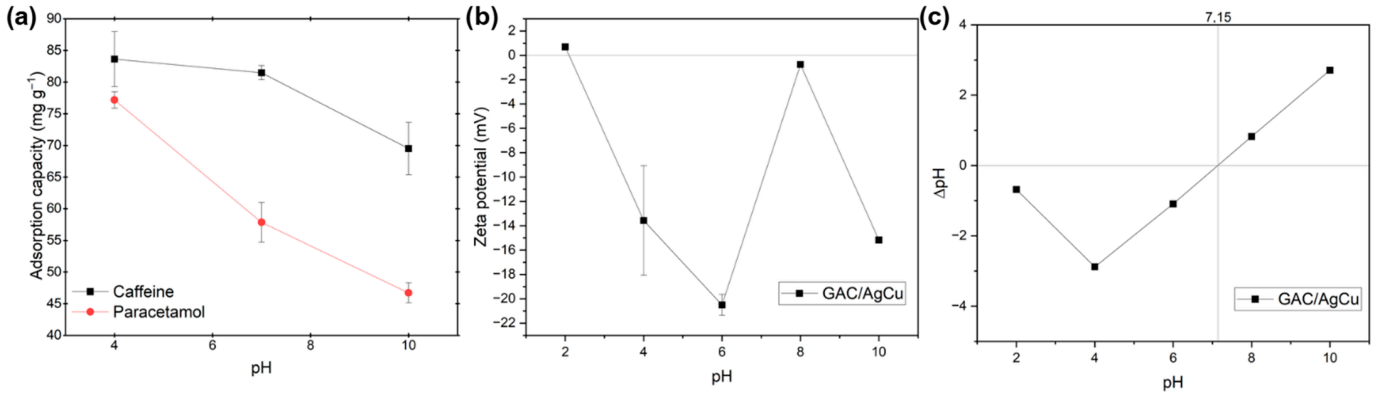

Figure 6. Effect of pH on contaminants adsorption (**a**); zeta potential analysis (**b**); and determination of pH_{PZC} (**c**). Experimental conditions: mass of GAC/AgCu = 0.01 g; temperature = 298 K; concentration = 30 mg L^{-1}.

From Figure 6a, in both cases the adsorption capacity is higher at an acidic medium of pH 4.0 (83.643 mg g^{-1} for caffeine and 77.188 mg g^{-1} for paracetamol), whereas at a basic medium of pH 10 the adsorption capacity is at its lowest (69.501 mg g^{-1} for caffeine and 46.710 mg g^{-1} for paracetamol). Figure 6b shows that GAC/AgCu possesses predominantly negative surface charges. Figure 6c shows the potential for zero charge of GAC and GAC/AgCu. According to Hermes et al. [69], pH_{PZC} indicates the pH value at which the charge balance is zero, providing information about the nature of the adsorbent and thus predicting existing electrostatic interactions. The results reveal a pH_{PZC} of 7.15 for GAC/AgCu indicating that below pH_{PZC} total surface charge balance, including the internal pore structure, are predominantly positively charged, favoring electrostatic attraction between the adsorbent and the adsorbates. On the other hand, at pH values above pH_{PZC}, the number of negative active sites predominates. It is worth mentioning that zeta potential reflects the electrokinetic charge at the shear plane of the particles, while pH_{PZC} identifies the pH where the net surface charge is neutral, hence the discrepancy between analyses.

The adsorption behavior of paracetamol (pKa 9.5) is significantly affected by the solution's pH [5]. Optimal adsorption occurs at acidic pH levels because paracetamol remains in its undissociated form (neutral), facilitating dispersion interactions between the adsorbent and the drug [70]. In contrast, at basic pH levels, the drug dissociates into anions, leading to weaker interactions with the negatively charged adsorbent surface as electrostatic repulsion occurs [71,72]. For caffeine (pKa = 10.4), the molecule remains non-ionic at pH levels between 4 and 7, which allows for electrostatic attraction between the adsorbent and the adsorbate [7,73].

The effect of adsorbent dosage on the adsorption capacity is shown in Figure 7. In both cases, a decrease in q_e was observed as the adsorbent dosage increased, while the overall removal percentage increased with dosage. This trend is commonly attributed to the fact that at lower dosages, the ratio of contaminant molecules to available adsorption sites is higher, leading to a more efficient saturation of the surface. As the adsorbent mass increases, the total number of active sites increases; however, many of these sites remain unsaturated or become less accessible due to the aggregation or overlapping of the adsorbent particles [5]. Furthermore, increasing the adsorbent dosage leads to a decrease in the adsorption capacity due to the mathematical relationship where the mass is in the denominator.

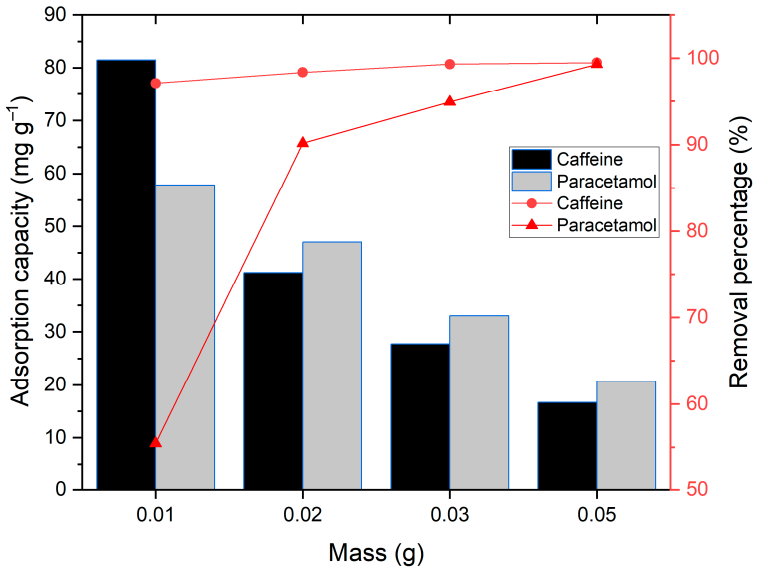

Figure 7. Effect of mass of GAC/AgCu on contaminants adsorption. Experimental conditions: pH = 7; temperature = 298 K; concentration = 30 mgL^{-1}.

The effects of contact time were evaluated through mathematical models, according to Figure 8. The model parameters obtained are shown in Table 2. For paracetamol, adsorption process reached a satisfactory equilibrium around 330 min at an adsorption capacity of 49.692 mg g^{-1}, for caffeine the capacity adsorption of 56.174 mg g^{-1} was reached at 210 min. For both contaminants, the models used well-adjusted to experimental data with a range of coefficient of determination (R^2) of 0.945–0.985. The pseudo-first-order was better fit for both contaminants with higher R^2. Similar results were found where authors indicated that the adsorption process involved a physisorption mechanism, where the interaction occurred through attraction forces on the surface of the adsorbent [74–77]. The slight deviations observed, particularly at longer contact times, are attributed to the linearized form of the pseudo-first-order model. As the system approaches equilibrium, the term $(q_e - q_t)$ becomes minimal, causing the logarithmic scale to amplify small experimental uncertainties or fluctuations in concentration measurements.

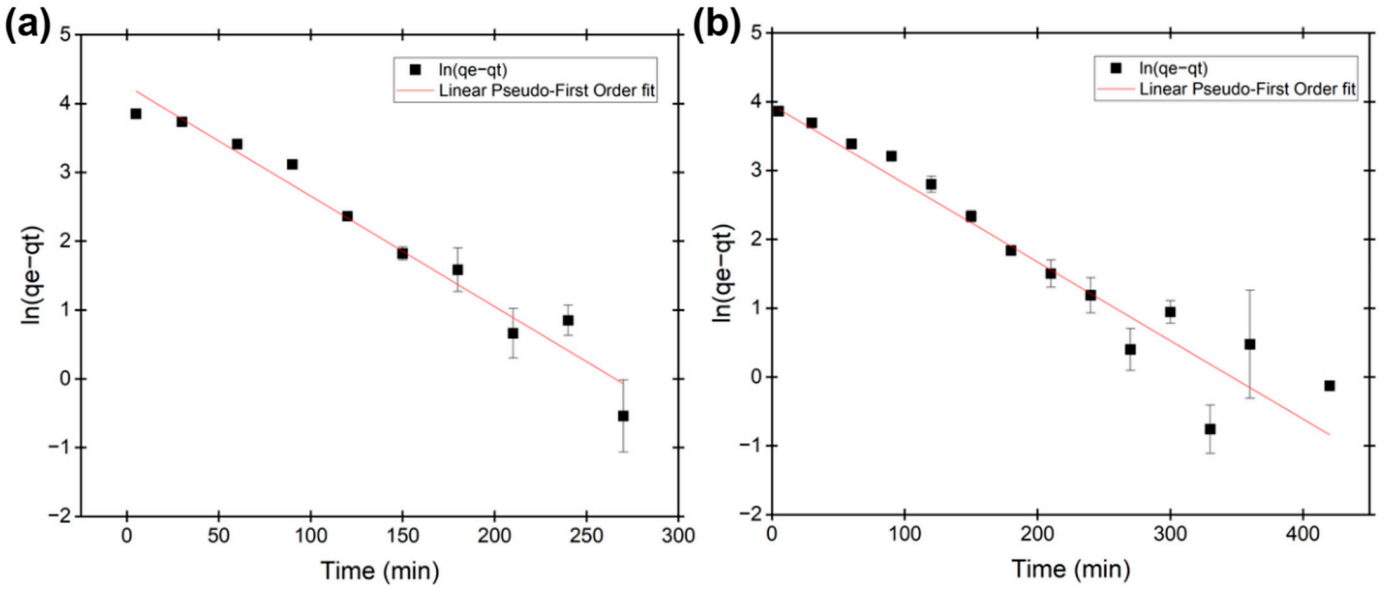

Figure 8. Caffeine (**a**) and paracetamol (**b**) adsorption kinetics by GAC/AgCu. Experimental conditions: mass of GAC/AgCu = 0.01 g; pH = 7; temperature = 298 K; concentration = 30 mg L^{-1}.

Table 2. Kinetic parameters of caffeine and paracetamol adsorption onto GAC/AgCu.

Kinetic Model	Parameters	Caffeine	Paracetamol
Pseudo-first-order	$q_{e,exp}$ (mg g^{-1})	56.174	49.692
	k_1 (min^{-1})	0.015	0.011
	R^2	0.985	0.975
	χ^2 [1]	11.328	3.582
	SSE [2]	0.878	2.282
Pseudo-second-order	$q_{e,calc}$ (mg g^{-1})	73.438	70.102
	k_2 (g mg^{-1} min^{-1})	1.597×10^{-4}	9.800×10^{-5}
	R^2	0.945	0.966
	χ^2	9.113	2.638
	SSE	1.048	1.793

[1] χ^2: statistic parameter, chi-squared. [2] SSE: statistic parameter, sum of squared errors.

The Langmuir, Freundlich and Temkin isotherm models were investigated to study the equilibrium adsorption characteristics of caffeine and paracetamol. The values of different model parameters at the used temperatures are given in Table 3. In both cases, the Langmuir model (Figure 9) showed better fitting of experimental data with higher values of R^2. The maximum adsorption capacity calculated by the Langmuir model was 138.350 mg g^{-1} for caffeine and 92.214 mg g^{-1} for paracetamol using the GAC/AgCu adsorbent at a temperature of 298 K. Furthermore, values of K_L and $1/n_F < 1$ indicate favorable adsorption for both contaminants [71,78]. Additionally, the maximum adsorption capacity decreases (q_{mL}) with temperature increase for caffeine, indicating an exothermic adsorption, whereas it increases with temperature increase for paracetamol, indicating an endothermic adsorption.

Table 3. Isotherm parameters of caffeine and paracetamol adsorption on GAC/AgCu.

		Caffeine			Paracetamol		
Model	**Parameters**	**298 K**	**308 K**	**318 K**	**298 K**	**308 K**	**318 K**
Langmuir	q_{mL} (mg g^{-1})	138.350	127.578	116.510	92.214	107.139	120.002
	K_L (L mg^{-1})	0.695	0.401	0.383	0.101	0.139	0.163
	R^2	0.999	0.998	0.999	0.990	0.995	0.993
	χ^2	4.284	4.601	1.542	2.485	2.224	4.879
	SSE	1.101×10^{-4}	3.282×10^{-4}	2.863×10^{-4}	0.005	0.002	0.002
Freundlich	K_F ((mg g^{-1})/(mg L^{-1})^{n_F})	43.209	32.902	29.413	11.8386	15.433	19.295
	n_F	2.653	2.468	2.492	1.978	1.968	2.035
	R^2	0.837	0.819	0.878	0.949	0.909	0.911
	χ^2	10,173.34	8707.267	7671.441	4197.545	5700.538	6845.871
	SSE	0.157	0.164	0.102	0.037	0.075	0.077
Temkin	b_T (g mol^{-1})	105.41	109.734	124.237	129.261	113.650	108.602
	K_T (L mg^{-1})	11.51	5.779	5.345	1.155	1.503	1.947
	R^2	0.938	0.947	0.957	0.954	0.961	0.950
	χ^2	13.028	11.258	5.764	6.718	4.613	6.283
	SSE	1100.761	724.002	484.556	250.406	314.136	4815.984

The fundamental premise of the Langmuir isotherm model is the absence of interaction between adsorbate molecules, leading to monolayer coverage on a surface with energetically identical active sites [76]. This stands in opposition to the Freundlich and Temkin models, which describe multilayer adsorption on heterogeneous surfaces with varying site energies [76,79]. Since the experimental data aligned more closely with the

Langmuir model, it can be inferred that the adsorption process on the GAC/AgCu surface occurs via a monolayer mechanism, indicating a high degree of surface homogeneity and uniform energy distribution among the active sites.

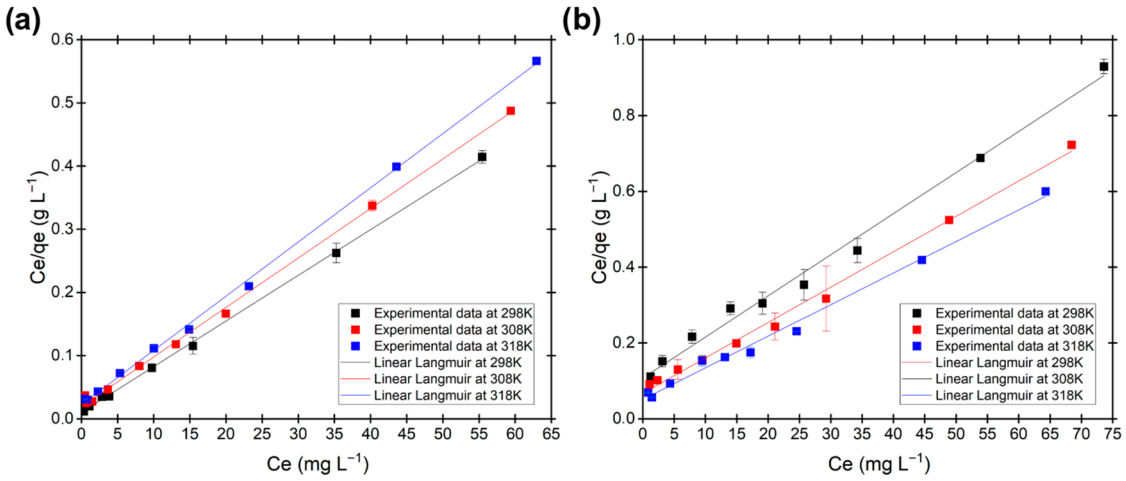

Figure 9. Caffeine (**a**) and paracetamol (**b**) adsorption isotherms by GAC/AgCu for linear Langmuir model. Experimental conditions: mass of GAC/AgCu = 0.01 g; pH = 7; concentration = 30 mg L^{-1}.

Comparison of caffeine and paracetamol adsorption capacity on GAC/AgCu with other adsorbents in the literature are shown in Table S1. The maximum adsorption capacity of the GAC/AgCu composite exhibits a moderate performance when compared to other adsorbents reported in the literature. As shown in Table S1, the values obtained in this work are lower than those of some non-modified materials, such as AC from olive stone. From a strict economic perspective, the requirement for metallic modification might appear as a disadvantage compared to higher-capacity, raw precursors. However, it is crucial to highlight that the incorporation of Ag/CuO nanoparticles provides the material with essential anti-microbial properties [42,43]. The reusability and economic viability of the GAC/AgCu adsorbent were evaluated through consecutive adsorption-desorption cycles (Figure S2). The regeneration was performed using tap water as the stripping agent. A progressive decline in removal efficiency was observed: caffeine maintained a removal rate above 50% for up to 4 cycles, whereas paracetamol's efficiency dropped more significantly after 2 cycles. This behavior suggests that while the material remains active, successive regenerative processes may lead to the partial blockage of pores or the irreversible occupation of high-energy active sites by the contaminants [80]. The higher stability observed for caffeine suggests a more reversible interaction with the surface compared to paracetamol. These findings indicate that while the adsorbent is reusable, further optimization of the desorption step with other stripping agents could potentially extend its operational lifespan.

Regarding the thermodynamic study, the equilibrium data from adsorption isotherm experiments were used to assess Gibbs free energy (ΔG°), enthalpy (ΔH°) and entropy (ΔS°), theoretically calculated by Equations (7)–(9) and shown in Table 4. The negative values of ΔG° confirm the spontaneous nature of the adsorption process, implying that the system reaches a more stable state without the need for external energy input under the evaluated experimental conditions. The change in enthalpy was -31.377 kJ mol^{-1} for caffeine pointing out the exothermic nature of its adsorption and 27.644 kJ mol^{-1} for paracetamol pointing out the endothermic nature of its adsorption, which are in agreement with the variation in the maximum adsorption capacity of each contaminant for the temperatures studied in the equilibrium isotherms tests. Furthermore, since $|\Delta H^\circ| < 40$ kJ mol^{-1} for both contaminants, it can be suggested that the adsorption process in this case involves physical

mechanisms [73,81]. Finally, the change in entropy (ΔS°) was −77.154 J $mol^{-1}K^{-1}$ for caffeine, indicating an increase in order during the absorption process at the solid-solution interface, whereas it was 103.925 J $mol^{-1}K^{-1}$ for paracetamol, indicating an increase in randomness on the adsorbent surface [82].

Table 4. Thermodynamic parameters of caffeine and paracetamol adsorption on GAC/AgCu.

Contaminant	Temperature (K)	ΔG° (kJ mol^{-1})	ΔH° (kJ mol^{-1})	ΔS° (J mol^{-1} K^{-1})
Caffeine	298	−8.524	−31.377	−77.154
	308	−7.317		
	318	−7.000		
Paracetamol	298	−3.332	27.644	103.925
	308	−4.421		
	318	−5.410		

3.3. Antibacterial Tests Results

The adsorption capacity of pure GAC and GAC/AgCu was studied using mass variation. The antibacterial tests were evaluated using *E. coli*. The results are shown in Figure 10. The smallest mass of material (0.01 g) showed a low percentage of bacterial reduction. On the other hand, the masses of 0.03 g and 0.09 g showed no significant difference, since both were effective against the bacteria under study, showing a reduction percentage of over 97%. GAC exhibited higher optical density values than the positive control, whose value was 0.612 (OD600), which suggests that the antibacterial effect of the material is related to the presence of silver and copper on the surface of the material, as they are antibacterial agents.

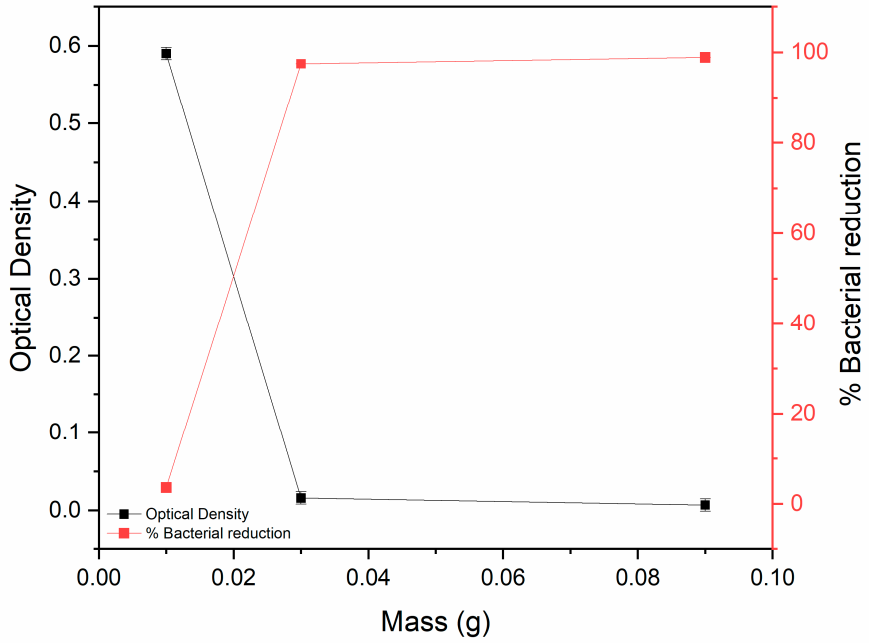

Figure 10. Influence of mass on the percentage reduction in *E. coli* in water.

According to Shivananda [43], although the exact mechanism of action of the effectiveness of antibacterial particles is unknown, the literature claims that silver ions influence *K*+ ions generated by bacteria. In addition, as reported by Morsi et al. [83], after entering bacterial cells, silver particles act to deactivate enzymes, causing the generation of hydrogen peroxide, which influences cell viability and causes bacterial death. The authors also point out that the mechanism of action of copper particles is similar to that of silver, which can

bind to DNA molecules and generate cross-linking disorders within and between nucleic acid chains, as well as stopping biochemical processes.

Studies carried out by Manikandan et al. [84] evaluated the hybrid effect of silver and copper against *E. coli* bacteria and showed a significant inhibitory capacity, corroborating the findings of this study. In this respect, the synergistic action of silver and copper may have contributed to the increase in antibacterial activity, since the electrostatic attraction between the silver and copper particles and the cell membrane favors antibacterial action [42], suggesting that the combination of the two agents makes the adsorbent more effective, as well as reducing the cost of silver, which is expensive. In this way, it is possible to highlight that the mass of modified material had an influence on obtaining a greater bacterial reduction capacity and that the material is a proposal with potential application for the treatment of contaminated water against *E. coli*.

4. Conclusions

Adsorbent GAC/AgCu has been successfully produced, characterized and used in adsorptive and antibacterial tests. The study identified pH 4 and a dosage of 0.01 g as optimal conditions, providing a baseline for scaling up the process. In the kinetic study, the pseudo-first-order model was the most suitable for both contaminants and equilibrium isothermal tests showed that the Langmuir model was the best fit suggesting that adsorption occurs via physisorption mechanism and takes place onto a more homogenous surface, with maximum adsorption capacity of 138.350 mg g^{-1} for caffeine and 92.214 mg g^{-1} for paracetamol. In addition, antibacterial tests showed that while unmodified GAC lacks inhibitory properties, the GAC/AgCu composite achieved a 97% reduction in E. coli activity. This confirms that Ag/Cu impregnation transforms a standard adsorbent into a potent antimicrobial agent, essential for preventing biofouling in water treatment systems. Although the comparison with other non-modified ACs highlighted only a moderate performance of GAC/AgCu on the adsorption of the contaminants, the integration of Ag and CuO nanoparticles enabled anti-microbial properties on the adsorbent. This dual functionality justifies the synthesis of GAC/AgCu, as it not only targets organic micro-pollutants but also prevents biological proliferation, a feature that standard activated carbons typically lack. Future technical-economic studies should be conducted to quantify these long-term benefits in large-scale systems.

Furthermore, based on the present findings, future research should optimize the synthesis of GAC/AgCu composites. This involves refining the concentration of modifiers to consequently preserve the adsorbent's specific surface area, thereby enhancing the adsorption capacity for organic pollutants while maintaining the antibacterial activity provided by the silver and copper. Additionally, in real-world applications, the adsorption of caffeine and paracetamol would occur in the presence of competing species, such as salts, mixed contaminants and natural organic matter. Thus, future studies should adopt a more complex and realistic medium for adsorption experiments. Finally, a more comprehensive study of the adsorption mechanisms, moving beyond the interpretation of kinetic data, is required to provide a deeper understanding of the governing processes.

Supplementary Materials: The following supporting information can be downloaded at: https://www.mdpi.com/article/10.3390/pr14061009/s1, Figure S1: FTIR spectrum of GAC and GAC/AgCu sample; Figure S2: Reuse test for the adsorption of caffeine and paracetamol on GAC/AgCu; Table S1: Comparison of caffeine and paracetamol adsorption capacity on GAC/AgCu. References [64,74,85–88] are cited in the Supplementary Materials.

Author Contributions: Methodology, L.C.A.M., J.F.R. and J.S.d.S.; investigation, L.C.A.M., J.F.R., J.S.d.S.; resources, S.R.L. and R.B.; writing—original draft preparation, L.C.A.M., J.F.R. and J.S.d.S.;

writing—review and editing, L.F.C., L.N. and R.B.; supervision, L.F.C., L.N., S.R.L. and R.B.; project administration, R.B. All authors have read and agreed to the published version of the manuscript.

Funding: This research was funded by Conselho Nacional de Desenvolvimento Científico e Tecnológico (CNPq), grant number 131626/2023-0, and Smart Research Laboratory. Also, Complex of Research Support Center of State University of Maringá (COMCAP) supplied technical support of the TEM and SEM analysis.

Data Availability Statement: Some datasets presented in this article are not readily available due to confidentiality and contractual agreements.

Conflicts of Interest: The authors declare no conflicts of interest.

References

1. dos Reis Oliveira, M.; Paulino, I.M.R.; Resende, J.F.; Simão, L.; Vieira, M.F.; Bergamasco, R.; Vieira, A.M.S. Valorization of Biomass Ash for the Effective Removal of Dipyrone from Water: An Efficient and Low-Cost Option. *J. Chem. Technol. Biotechnol.* **2023**, *98*, 1690–1702. [CrossRef]
2. Ashiwaju, B.I.; Uzougbo, C.G.; Orikpete, O.F. Environmental Impact of Pharmaceuticals: A Comprehensive Review. *Matrix Sci. Pharma* **2023**, *7*, 85–94. [CrossRef]
3. Thiebault, T.; Chassiot, L.; Fougère, L.; Destandau, E.; Simonneau, A.; Van Beek, P.; Souhaut, M.; Chapron, E. Record of Pharmaceutical Products in River Sediments: A Powerful Tool to Assess the Environmental Impact of Urban Management? *Anthropocene* **2017**, *18*, 47–56. [CrossRef]
4. Wang, K.; Zhuang, T.; Su, Z.; Chi, M.; Wang, H. Antibiotic Residues in Wastewaters from Sewage Treatment Plants and Pharmaceutical Industries: Occurrence, Removal and Environmental Impacts. *Sci. Total Environ.* **2021**, *788*, 147811. [CrossRef] [PubMed]
5. Lee, W.J.; Goh, P.S.; Lau, W.J.; Ismail, A.F. Removal of Pharmaceutical Contaminants from Aqueous Medium: A State-of-the-Art Review Based on Paracetamol. *Arab. J. Sci. Eng.* **2020**, *45*, 7109–7135. [CrossRef]
6. Alhassen, H.M.; Dyer, F.J.; Thompson, R.M. The Photolytic Breakdown of Caffeine and Paracetamol Residues in Surface Water. *Water Environ. Res.* **2023**, *95*, e10909. [CrossRef] [PubMed]
7. dos Santos, D.F.; Moreira, W.M.; de Araújo, T.P.; Bergamasco, R.; Ostroski, I.C.; de Barros, M.A.S.D. Non-Conventional Processes Applied for the Removal of Pharmaceutics Compounds in Waters: A Review. *Process Saf. Environ. Prot.* **2022**, *167*, 527–542. [CrossRef]
8. Borrull, J.; Colom, A.; Fabregas, J.; Borrull, F.; Pocurull, E. Presence, Behaviour and Removal of Selected Organic Micropollutants Through Drinking Water Treatment. *Chemosphere* **2021**, *276*, 130023. [CrossRef]
9. Mestre, A.S.; Bexiga, A.S.; Proença, M.; Andrade, M.; Pinto, M.L.; Matos, I.; Fonseca, I.M.; Carvalho, A.P. Activated Carbons from Sisal Waste by Chemical Activation with K_2CO_3: Kinetics of Paracetamol and Ibuprofen Removal from Aqueous Solution. *Bioresour. Technol.* **2011**, *102*, 8253–8260. [CrossRef]
10. Vymazal, J.; Březinová, T.D.; Koželuh, M.; Kule, L. Occurrence and Removal of Pharmaceuticals in Four Full-Scale Constructed Wetlands in the Czech Republic—The First Year of Monitoring. *Ecol. Eng.* **2017**, *98*, 354–364. [CrossRef]
11. Guruge, K.S.; Goswami, P.; Tanoue, R.; Nomiyama, K.; Wijesekara, R.G.S.; Dharmaratne, T.S. First Nationwide Investigation and Environmental Risk Assessment of 72 Pharmaceuticals and Personal Care Products from Sri Lankan Surface Waterways. *Sci. Total Environ.* **2019**, *690*, 683–695. [CrossRef]
12. Ebele, A.J.; Oluseyi, T.; Drage, D.S.; Harrad, S.; Abdallah, M.A.-E. Occurrence, Seasonal Variation and Human Exposure to Pharmaceuticals and Personal Care Products in Surface Water, Groundwater and Drinking Water in Lagos State, Nigeria. *Emerg. Contam.* **2020**, *6*, 124–132. [CrossRef]
13. Zhang, Y.; Rashid, A.; Guo, S.; Jing, Y.; Zeng, Q.; Li, Y.; Adyari, B.; Yang, J.; Tang, L.; Yu, C.-P.; et al. Spatial Autocorrelation and Temporal Variation of Contaminants of Emerging Concern in a Typical Urbanizing River. *Water Res.* **2022**, *212*, 118120. [CrossRef] [PubMed]
14. de Jesus Silva Chaves, M.; Barbosa, S.C.; de Melo Malinowski, M.; Volpato, D.; Castro, Í.B.; dos Santos Franco, T.C.R.; Primel, E.G. Pharmaceuticals and Personal Care Products in a Brazilian Wetland of International Importance: Occurrence and Environmental Risk Assessment. *Sci. Total Environ.* **2020**, *734*, 139374. [CrossRef] [PubMed]
15. Gardinali, P.R.; Zhao, X. Trace Determination of Caffeine in Surface Water Samples by Liquid Chromatography–Atmospheric Pressure Chemical Ionization–Mass Spectrometry (LC–APCI–MS). *Environ. Int.* **2002**, *28*, 521–528. [CrossRef]
16. Li, S.; He, B.; Wang, J.; Liu, J.; Hu, X. Risks of Caffeine Residues in the Environment: Necessity for a Targeted Ecopharmacovigilance Program. *Chemosphere* **2020**, *243*, 125343. [CrossRef]

17. Hillebrand, O.; Nödler, K.; Licha, T.; Sauter, M.; Geyer, T. Caffeine as an Indicator for the Quantification of Untreated Wastewater in Karst Systems. *Water Res.* **2012**, *46*, 395–402. [CrossRef]
18. Phukan, D.; Kumar, V. Tracking Drugged Waters from Various Sources to Drinking Water—Its Persistence, Environmental Risk Assessment, and Removal Techniques. *Environ. Sci. Pollut. Res.* **2023**, *30*, 86676–86698. [CrossRef]
19. Vázquez-Tapia, I.; Salazar-Martínez, T.; Acosta-Castro, M.; Meléndez-Castolo, K.A.; Mahlknecht, J.; Cervantes-Avilés, P.; Capparelli, M.V.; Mora, A. Occurrence of Emerging Organic Contaminants and Endocrine Disruptors in Different Water Compartments in Mexico—A Review. *Chemosphere* **2022**, *308*, 136285. [CrossRef]
20. Duarte, I.A.; Reis-Santos, P.; Fick, J.; Cabral, H.N.; Duarte, B.; Fonseca, V.F. Neuroactive Pharmaceuticals in Estuaries: Occurrence and Tissue-Specific Bioaccumulation in Multiple Fish Species. *Environ. Pollut.* **2023**, *316*, 120531. [CrossRef]
21. Dulsat-Masvidal, M.; Ciudad, C.; Infante, O.; Mateo, R.; Lacorte, S. Water Pollution Threats in Important Bird and Biodiversity Areas from Spain. *J. Hazard. Mater.* **2023**, *448*, 130938. [CrossRef] [PubMed]
22. Lima, D.R.S.; Tonucci, M.C.; Libânio, M.; Aquino, S.F. De Fármacos e Desreguladores Endócrinos Em Águas Brasileiras: Ocorrência e Técnicas de Remoção. *Eng. Sanit. E Ambient.* **2017**, *22*, 1043–1054. [CrossRef]
23. An, J.; Zhou, Q.; Sun, F.; Zhang, L. Ecotoxicological Effects of Paracetamol on Seed Germination and Seedling Development of Wheat (*Triticum Aestivum* L.). *J. Hazard. Mater.* **2009**, *169*, 751–757. [CrossRef] [PubMed]
24. Daniel, D.; Dionísio, R.; de Alkimin, G.D.; Nunes, B. Acute and Chronic Effects of Paracetamol Exposure on Daphnia Magna: How Oxidative Effects May Modulate Responses at Distinct Levels of Organization in a Model Species. *Environ. Sci. Pollut. Res.* **2019**, *26*, 3320–3329. [CrossRef]
25. Pires, A.; Almeida, Â.; Correia, J.; Calisto, V.; Schneider, R.J.; Esteves, V.I.; Soares, A.M.V.M.; Figueira, E.; Freitas, R. Long-Term Exposure to Caffeine and Carbamazepine: Impacts on the Regenerative Capacity of the Polychaete *Diopatra neapolitana*. *Chemosphere* **2016**, *146*, 565–573. [CrossRef]
26. Pires, A.; Almeida, Â.; Calisto, V.; Schneider, R.J.; Esteves, V.I.; Wrona, F.J.; Soares, A.M.V.M.; Figueira, E.; Freitas, R. Long-Term Exposure of Polychaetes to Caffeine: Biochemical Alterations Induced in *Diopatra neapolitana* and *Arenicola marina*. *Environ. Pollut.* **2016**, *214*, 456–463. [CrossRef]
27. Pires, A.; Almeida, Â.; Calisto, V.; Schneider, R.J.; Esteves, V.I.; Wrona, F.J.; Soares, A.M.V.M.; Figueira, E.; Freitas, R. *Hediste diversicolor* as Bioindicator of Pharmaceutical Pollution: Results from Single and Combined Exposure to Carbamazepine and Caffeine. *Comp. Biochem. Physiol. Part C Toxicol. Pharmacol.* **2016**, *188*, 30–38. [CrossRef]
28. Aguirre-Martínez, G.V.; André, C.; Gagné, F.; Martín-Díaz, L.M. The Effects of Human Drugs in *Corbicula fluminea*. Assessment of Neurotoxicity, Inflammation, Gametogenic Activity, and Energy Status. *Ecotoxicol. Environ. Saf.* **2018**, *148*, 652–663. [CrossRef]
29. Pennington, M.J.; Rothman, J.A.; Jones, M.B.; McFrederick, Q.S.; Gan, J.; Trumble, J.T. Effects of Contaminants of Emerging Concern on *Megaselia scalaris* (Lowe, Diptera: Phoridae) and Its Microbial Community. *Sci. Rep.* **2017**, *7*, 8165. [CrossRef]
30. Januário, E.F.D.; Fachina, Y.J.; Wernke, G.; Demiti, G.M.M.; Beltran, L.B.; Bergamasco, R.; Vieira, A.M.S. Application of Activated Carbon Functionalized with Graphene Oxide for Efficient Removal of COVID-19 Treatment-Related Pharmaceuticals from Water. *Chemosphere* **2022**, *289*, 133213. [CrossRef] [PubMed]
31. Srivastava, A.; Gupta, B.; Majumder, A.; Gupta, A.K.; Nimbhorkar, S.K. A Comprehensive Review on the Synthesis, Performance, Modifications, and Regeneration of Activated Carbon for the Adsorptive Removal of Various Water Pollutants. *J. Environ. Chem. Eng.* **2021**, *9*, 106177. [CrossRef]
32. Almeida-Naranjo, C.E.; Guerrero, V.H.; Villamar-Ayala, C.A. Emerging Contaminants and Their Removal from Aqueous Media Using Conventional/Non-Conventional Adsorbents: A Glance at the Relationship Between Materials, Processes, and Technologies. *Water* **2023**, *15*, 1626. [CrossRef]
33. Vidovix, T.B.; Quesada, H.B.; Bergamasco, R.; Vieira, M.F.; Vieira, A.M.S. Adsorption of Safranin-O Dye by Copper Oxide Nanoparticles Synthesized from *Punica granatum* Leaf Extract. *Environ. Technol.* **2022**, *43*, 3047–3063. [CrossRef]
34. Bazana, S.L.; Shimabuku-Biadola, Q.L.; Arakawa, F.S.; Gomes, R.G.; Cossich, E.S.; Bergamasco, R. Modified Activated Carbon with Silver–Copper Mixed Oxides Nanoparticles for Removal of Heavy Metals from Water. *Int. J. Environ. Sci. Technol.* **2019**, *16*, 6727–6734. [CrossRef]
35. Paixão, R.M.; Reck, I.M.; Bergamasco, R.; Vieira, M.F.; Vieira, A.M.S. Activated Carbon of Babassu Coconut Impregnated with Copper Nanoparticles by Green Synthesis for the Removal of Nitrate in Aqueous Solution. *Environ. Technol.* **2018**, *39*, 1994–2003. [CrossRef]
36. Wernke, G.; Fagundes-Klen, M.R.; Vieira, M.F.; Suzaki, P.Y.R.; Souza, H.K.S.d.e.; Shimabuku, Q.L.; Bergamasco, R. Mathematical Modelling Applied to the Rate-Limiting Mass Transfer Step Determination of a Herbicide Biosorption onto Fixed-Bed Columns. *Environ. Technol.* **2020**, *41*, 638–648. [CrossRef] [PubMed]
37. Wernke, G.; Silva, M.F.; da Silva, E.A.; Fagundes-Klen, M.R.; Suzaki, P.Y.R.; Triques, C.C.; Bergamasco, R. Ag and CuO Nanoparticles Decorated on Graphene Oxide/Activated Carbon as a Novel Adsorbent for the Removal of Cephalexin from Water. *Colloids Surf. A Physicochem. Eng. Asp.* **2021**, *627*, 127203. [CrossRef]

38. Andrade, M.B.; Santos, T.R.T.; Guerra, A.C.S.; Silva, M.F.; Demiti, G.M.M.; Bergamasco, R. Evaluation of Magnetic Nano Adsorbent Produced from Graphene Oxide with Iron and Cobalt Nanoparticles for Caffeine Removal from Aqueous Medium. *Chem. Eng. Process.—Process Intensif.* **2022**, *170*, 108694. [CrossRef]
39. Pirvu, F.; Covaliu-Mierlă, C.I.; Catrina, G.A. Removal of Acetaminophen Drug from Wastewater by Fe_3O_4 and ZSM-5 Materials. *Nanomaterials* **2023**, *13*, 1745. [CrossRef]
40. Biswas, P.; Bandyopadhyaya, R. Synergistic Antibacterial Activity of a Combination of Silver and Copper Nanoparticle Impregnated Activated Carbon for Water Disinfection. *Environ. Sci. Nano* **2017**, *4*, 2405–2417. [CrossRef]
41. Shimabuku, Q.L.; Arakawa, F.S.; Silva, M.F.; Coldebella, P.F.; Ueda-Nakamura, T.; Fagundes-Klen, M.R.; Bergamasco, R. Water Treatment with Exceptional Virus Inactivation Using Activated Carbon Modified with Silver (Ag) and Copper Oxide (CuO) Nanoparticles. *Environ. Technol.* **2017**, *38*, 2058–2069. [CrossRef]
42. Videira-Quintela, D.; Guillén, F.; Montalvo, G.; Martin, O. Silver, Copper, and Copper Hydroxy Salt Decorated Fumed Silica Hybrid Composites as Antibacterial Agents. *Colloids Surf. B Biointerfaces* **2020**, *195*, 111216. [CrossRef]
43. Shivananda, C.S. Silk Fibroin-Based Green Colloidal Silver Nanoparticle Synthesis and Their Antibacterial and Anticancer Properties. *Inorg. Chem. Commun.* **2023**, *158*, 111611. [CrossRef]
44. Jolivet, J.-P.; Cassaignon, S.; Chanéac, C.; Chiche, D.; Durupthy, O.; Portehault, D. Design of Metal Oxide Nanoparticles: Control of Size, Shape, Crystalline Structure and Functionalization by Aqueous Chemistry. *Comptes Rendus Chim.* **2010**, *13*, 40–51. [CrossRef]
45. Ahmed, N.S.; Menzel, R.; Wang, Y.; Garcia-Gallastegui, A.; Bawaked, S.M.; Obaid, A.Y.; Basahel, S.N.; Mokhtar, M. Graphene-Oxide-Supported CuAl and CoAl Layered Double Hydroxides as Enhanced Catalysts for Carbon-Carbon Coupling via Ullmann Reaction. *J. Solid State Chem.* **2017**, *246*, 130–137. [CrossRef]
46. Sun, L.; Zhao, Z.; Sun, Y.; Wang, X.; Liu, X.; Yang, Y.; Qiu, J. Activated Coal-Based Graphene with Hierarchical Porous Structures for Ultra-High Energy Density Supercapacitors. *Diam. Relat. Mater.* **2020**, *106*, 107827. [CrossRef]
47. Zamorska, J.; Kiełb-Sotkiewicz, I. UV Radiation in Wastewater Disinfection. In *Proceedings of CEE 2023*; Blikharskyy, Z., Koszelnik, P., Lichołai, L., Nazarko, P., Katunský, D., Eds.; Springer Nature: Cham, Switzerland, 2024; pp. 510–520. [CrossRef]
48. Thuptimdang, P.; Siripattanakul-Ratpukdi, S.; Ratpukdi, T.; Youngwilai, A.; Khan, E. Biofiltration for Treatment of Recent Emerging Contaminants in Water: Current and Future Perspectives. *Water Environ. Res.* **2021**, *93*, 972–992. [CrossRef]
49. Arakawa, F.S.; Shimabuku-Biadola, Q.L.; de Lima Bazana, S.; Silva, M.F.; de Abreu Filho, B.A.; Bergamasco, R. Activated Carbon Impregnation with Ag and Cu Composed Nanoparticles for *Escherichia coli* Contaminated Water Treatment. *Can. J. Chem. Eng.* **2019**, *97*, 2408–2418. [CrossRef]
50. Lagergren, S. Zur Theorie Der Sogenannten Adsorption Gelöster Stoffe. *Z. Chem. Ind. Kolloide* **1898**, *2*, 1–39.
51. Ho, Y.S.; McKay, G. Kinetic Models for the Sorption of Dye from Aqueous Solution by Wood. *Process Saf. Environ. Prot.* **1998**, *76*, 183–191. [CrossRef]
52. Armbruster, M.H.; Austin, J.B. The Adsorption of Gases on Plane Surfaces of Mica. *J. Am. Chem. Soc.* **1938**, *60*, 467–475. [CrossRef]
53. Freundlich, H. Über Die Adsorption in Lösungen. *Z. Phys. Chem.* **1907**, *57U*, 385–470. [CrossRef]
54. Musah, M.; Azeh, Y.; Mathew, J.; Umar, M.; Abdulhamid, Z.; Muhammad, A. Adsorption Kinetics and Isotherm Models: A Review. *Caliphate J. Sci. Technol.* **2022**, *4*, 20–26. [CrossRef]
55. Jiang, L.; Jia, Z.; Xu, X.; Chen, Y.; Peng, W.; Zhang, J.; Wang, H.; Li, S.; Wen, J. Preparation of Antimicrobial Activated Carbon Fiber by Loading with Silver Nanoparticles. *Colloids Surf. A Physicochem. Eng. Asp.* **2022**, *633*, 127868. [CrossRef]
56. Zhao, Y.; Wang, Z.Q.; Zhao, X.; Li, W.; Liu, S.X. Antibacterial Action of Silver-Doped Activated Carbon Prepared by Vacuum Impregnation. *Appl. Surf. Sci.* **2013**, *266*, 67–72. [CrossRef]
57. Mishra, S.P.; Ghosh, M.R. Use of Silver Impregnated Activated Carbon (SAC) for Cr(VI) Removal. *J. Environ. Chem. Eng.* **2020**, *8*, 103641. [CrossRef]
58. Shimabuku-Biadola, Q.L.; Arakawa, F.S.; Nishi, L.; Wernke, G.; Cusioli, L.F.; Bergamasco, R. Activated Carbon Impregnated with Ag(0) and Cu Oxides for the Removal of *Escherichia coli*, Giardia, and Cryptosporidium (Oo)Cysts from Water. *Desalination Water Treat.* **2024**, *317*, 100142. [CrossRef]
59. Xin, S.; Yang, H.; Chen, Y.; Yang, M.; Chen, L.; Wang, X.; Chen, H. Chemical Structure Evolution of Char During the Pyrolysis of Cellulose. *J. Anal. Appl. Pyrolysis* **2015**, *116*, 263–271. [CrossRef]
60. Rathinavel, S.; Saravanakumar, S.S. Synthesis of Silver Nanoparticles Through Orange Peel Powder for Antibacterial Composite Filler Applications. *J. Polym. Environ.* **2022**, *30*, 1407–1414. [CrossRef]
61. Ansari, A.R.; Ansari, S.A.; Parveen, N.; Ansari, M.O.; Osman, Z. Ag Nanoparticles Anchored Reduced Graphene Oxide Sheets@nickel Oxide Nanoflakes Nanocomposites for Enhanced Capacitive Performance of Supercapacitors. *Inorg. Chem. Commun.* **2023**, *150*, 110519. [CrossRef]
62. Foo, K.Y.; Hameed, B.H. Factors Affecting the Carbon Yield and Adsorption Capability of the Mangosteen Peel Activated Carbon Prepared by Microwave Assisted K_2CO_3 Activation. *Chem. Eng. J.* **2012**, *180*, 66–74. [CrossRef]
63. Lalhmunsiama; Lee, S.M.; Choi, S.S.; Tiwari, D. Simultaneous Removal of Hg(II) and Phenol Using Functionalized Activated Carbon Derived from Areca Nut Waste. *Metals* **2017**, *7*, 248. [CrossRef]

64. Gatrouni, M.; Asses, N.; Bedia, J.; Belver, C.; Molina, C.B.; Mzoughi, N. Acetaminophen Adsorption on Carbon Materials from Citrus Waste. *C-J. Carbon Res.* **2024**, *10*, 53. [CrossRef]
65. Depci, T. Comparison of Activated Carbon and Iron Impregnated Activated Carbon Derived from Gölbaşi Lignite to Remove Cyanide from Water. *Chem. Eng. J.* **2012**, *181–182*, 467–478. [CrossRef]
66. Resende, J.F.; Paulino, I.M.R.; dos Reis Oliveira, M.; Ferri, B.B.; Bergamasco, R.; Guilherme, M.R.; Rinaldi, A.W.; Vieira, A.M.S. Synthesis of Hydrogels from Fractionated Proteins of *Moringa oleifera* Lam. Seeds for the Treatment of Water Contaminated with Black Reactive Dye 5. *Can. J. Chem. Eng.* **2024**, *102*, 685–702. [CrossRef]
67. de Sousa, J.S.; de Oliveira, A.M.; do Nascimento, N.N.; Bergamasco, R.; de Abreu Filho, B.A.; Salcedo Vieira, A.M. Metal Nanoparticles in Flaxseed and Orange Waste: Sustainable Applications as Antimicrobial Agents in Water Treatment Systems. *Environ. Nanotechnol. Monit. Manag.* **2024**, *22*, 101024. [CrossRef]
68. Terzyk, A.P. The Influence of Activated Carbon Surface Chemical Composition on the Adsorption of Acetaminophen (Paracetamol) In Vitro. *Colloids Surf. A Physicochem. Eng. Asp.* **2001**, *177*, 23–45. [CrossRef]
69. Hermes, C.E.C.; dos Santos, D.F.; da Silva Fonseca, B.C.; Fonseca, I.M.; Quesada, H.B.; de Barros, M.A.S.D.; de Araújo, T.P. Multivariable Optimization of Activated Carbon Derived from Sapucaia (*Lecythis pisonis*) Shells for Enhanced Acetaminophen Adsorption. *Mater. Sci. Eng. B* **2026**, *328*, 119356. [CrossRef]
70. Spaltro, A.; Pila, M.N.; Colasurdo, D.D.; Noseda Grau, E.; Román, G.; Simonetti, S.; Ruiz, D.L. Removal of Paracetamol from Aqueous Solution by Activated Carbon and Silica. Experimental and Computational Study. *J. Contam. Hydrol.* **2021**, *236*, 103739. [CrossRef]
71. Sajid, M.; Bari, S.; Saif Ur Rehman, M.; Ashfaq, M.; Guoliang, Y.; Mustafa, G. Adsorption Characteristics of Paracetamol Removal onto Activated Carbon Prepared from *Cannabis sativum Hemp*. *Alex. Eng. J.* **2022**, *61*, 7203–7212. [CrossRef]
72. Kerkhoff, C.M.; da Boit Martinello, K.; Franco, D.S.P.; Netto, M.S.; Georgin, J.; Foletto, E.L.; Piccilli, D.G.A.; Silva, L.F.O.; Dotto, G.L. Adsorption of Ketoprofen and Paracetamol and Treatment of a Synthetic Mixture by Novel Porous Carbon Derived from *Butia capitata* Endocarp. *J. Mol. Liq.* **2021**, *339*, 117184. [CrossRef]
73. Bachmann, S.A.L.; Calvete, T.; Féris, L.A. Caffeine Removal from Aqueous Media by Adsorption: An Overview of Adsorbents Evolution and the Kinetic, Equilibrium and Thermodynamic Studies. *Sci. Total Environ.* **2021**, *767*, 144229. [CrossRef]
74. Preglo, A.R.; Namata, J.; Caculba, J.; Sanchez, G.; Joyno, C.; Pagalan, E.; Arazo, R.O. Paracetamol Removal from Aqueous Solution Through Activated Carbon from Mango Seeds. *Chem. Afr.* **2023**, *6*, 699–710. [CrossRef]
75. Quesada, H.B.; Cusioli, L.F.; de OBezerra, C.; Baptista, A.T.A.; Nishi, L.; Gomes, R.G.; Bergamasco, R. Acetaminophen Adsorption Using a Low-Cost Adsorbent Prepared from Modified Residues of *Moringa oleifera* Lam. Seed Husks. *J. Chem. Technol. Biotechnol.* **2019**, *94*, 3147–3157. [CrossRef]
76. Almeida-Naranjo, C.E.; Aldás, M.B.; Cabrera, G.; Guerrero, V.H. Caffeine Removal from Synthetic Wastewater Using Magnetic Fruit Peel Composites: Material Characterization, Isotherm and Kinetic Studies. *Environ. Chall.* **2021**, *5*, 100343. [CrossRef]
77. Bahrami, M.; Amiri, M.J.; Mahmoudi, M.R.; Zare, A. Statistical and Mathematical Modeling for Predicting Caffeine Removal from Aqueous Media by Rice Husk-Derived Activated Carbon. *Sustainability* **2023**, *15*, 7366. [CrossRef]
78. Baccar, R.; Sarrà, M.; Bouzid, J.; Feki, M.; Blánquez, P. Removal of Pharmaceutical Compounds by Activated Carbon Prepared from Agricultural By-Product. *Chem. Eng. J.* **2012**, *211–212*, 310–317. [CrossRef]
79. Somashekara, D.; Mulky, L. Sequestration of Contaminants from Wastewater: A Review of Adsorption Processes. *ChemBioEng Rev.* **2023**, *10*, 491–509. [CrossRef]
80. Das, T.K.; Ghosh, S.K.; Das, N.C. Green Synthesis of a Reduced Graphene Oxide/Silver Nanoparticles-Based Catalyst for Degradation of a Wide Range of Organic Pollutants. *Nano-Struct. Nano-Objects* **2023**, *34*, 100960. [CrossRef]
81. Nguyen, D.T.; Tran, H.N.; Juang, R.S.; Dat, N.D.; Tomul, F.; Ivanets, A.; Woo, S.H.; Hosseini-Bandegharaei, A.; Nguyen, V.P.; Chao, H.P. Adsorption Process and Mechanism of Acetaminophen onto Commercial Activated Carbon. *J. Environ. Chem. Eng.* **2020**, *8*, 104408. [CrossRef]
82. Anastopoulos, I.; Kyzas, G.Z. Are the Thermodynamic Parameters Correctly Estimated in Liquid-Phase Adsorption Phenomena? *J. Mol. Liq.* **2016**, *218*, 174–185. [CrossRef]
83. Morsi, R.E.; Alsabagh, A.M.; Nasr, S.A.; Zaki, M.M. Multifunctional Nanocomposites of Chitosan, Silver Nanoparticles, Copper Nanoparticles and Carbon Nanotubes for Water Treatment: Antimicrobial Characteristics. *Int. J. Biol. Macromol.* **2017**, *97*, 264–269. [CrossRef] [PubMed]
84. Manikandan, D.B.; Arumugam, M.; Sridhar, A.; Perumalsamy, B.; Ramasamy, T. Sustainable Fabrication of Hybrid Silver-Copper Nanocomposites (Ag-CuO NCs) Using *Ocimum americanum* L. as an Effective Regime against Antibacterial, Anticancer, Photocatalytic Dye Degradation and Microalgae Toxicity. *Environ. Res.* **2023**, *228*, 115867. [CrossRef]
85. Crespo, L.H.S.; Dutra, L.P.; Andrade, A.A.R.; Silva, T.L.; Spessato, L.; Cazetta, A.L.; Yamelit, M.E.N.; Ramos, L.M.M.; Pacheco, H.G.J.; Almeida, V.C. Comparative Study of the Adsorption Mechanisms of Caffeine and Remazol Brilliant Blue R Dye on Activated Carbon from Alpaca Fiber Residue. *Biomass Convers. Biorefinery* **2025**, *15*, 25307–25322. [CrossRef]

86. Medina, F.M.O.; Aguiar, M.B.; Parolo, M.E.; Avena, M.J. Insights of Competitive Adsorption on Activated Carbon of Binary Caffeine and Diclofenac Solutions. *J. Environ. Manag.* **2021**, *278*, 111523. [CrossRef] [PubMed]
87. dos Santos, D.; Moreira, W.; de Araújo, T.; Bernardo, M.; Fonseca, I.; Ostroski, I.; de Barros, M.A. Removal of Emerging Contaminants from Water by Using Carbon Materials Derived from Tingui Shells. *Separations* **2024**, *11*, 215. [CrossRef]
88. Pereira, L.; Castillo, V.; Calero, M.; González-Egido, S.; Martín-Lara, M.Á.; Solís, R.R. Promoting the Circular Economy: Valorization of a Residue from Industrial Char to Activated Carbon with Potential Environmental Applications as Adsorbents. *J. Environ. Manag.* **2024**, *356*, 120753. [CrossRef]

Disclaimer/Publisher's Note: The statements, opinions and data contained in all publications are solely those of the individual author(s) and contributor(s) and not of MDPI and/or the editor(s). MDPI and/or the editor(s) disclaim responsibility for any injury to people or property resulting from any ideas, methods, instructions or products referred to in the content.